Unfolding linac photon spectra and incident electron energies from experimental transmission data, with direct independent validation

E. S. M. Ali[a)]
Carleton Laboratory for Radiotherapy Physics, Department of Physics, Carleton University, 1125 Colonel By Drive, Ottawa, Ontario K1S 5B6, Canada

M. R. McEwen[b)]
Ionizing Radiation Standards, Institute for National Measurement Standards, National Research Council, M-35 Montreal Road, Ottawa, Ontario K1A 0R5, Canada

D. W. O. Rogers[c)]
Carleton Laboratory for Radiotherapy Physics, Department of Physics, Carleton University, 1125 Colonel By Drive, Ottawa, Ontario K1S 5B6, Canada

(Received 7 May 2012; revised 2 September 2012; accepted for publication 4 September 2012; published 9 October 2012)

Purpose: In a recent computational study, an improved physics-based approach was proposed for unfolding linac photon spectra and incident electron energies from transmission data. In this approach, energy differentiation is improved by simultaneously using transmission data for multiple attenuators and detectors, and the unfolding robustness is improved by using a four-parameter functional form to describe the photon spectrum. The purpose of the current study is to validate this approach experimentally, and to demonstrate its application on a typical clinical linac.
Methods: The validation makes use of the recent transmission measurements performed on the Vickers research linac of National Research Council Canada. For this linac, the photon spectra were previously measured using a NaI detector, and the incident electron parameters are independently known. The transmission data are for eight beams in the range 10–30 MV using thick Be, Al and Pb bremsstrahlung targets. To demonstrate the approach on a typical clinical linac, new measurements are performed on an Elekta *Precise* linac for 6, 10 and 25 MV beams. The different experimental setups are modeled using `EGSnrc`, with the newly added photonuclear attenuation included.
Results: For the validation on the research linac, the 95% confidence bounds of the unfolded spectra fall within the noise of the NaI data. The unfolded spectra agree with the `EGSnrc` spectra (calculated using independently known electron parameters) with RMS energy fluence deviations of 4.5%. The accuracy of unfolding the incident electron energy is shown to be ~3%. A transmission cutoff of only 10% is suitable for accurate unfolding, provided that the other components of the proposed approach are implemented. For the demonstration on a clinical linac, the unfolded incident electron energies and their 68% confidence bounds for the 6, 10 and 25 MV beams are 6.1 ± 0.1, 9.3 ± 0.1, and 19.3 ± 0.2 MeV, respectively. The unfolded spectra for the clinical linac agree with the `EGSnrc` spectra (calculated using the unfolded electron energies) with RMS energy fluence deviations of 3.7%. The corresponding measured and `EGSnrc`-calculated transmission data agree within 1.5%, where the typical transmission measurement uncertainty on the clinical linac is 0.4% (not including the uncertainties on the incident electron parameters).
Conclusions: The approach proposed in an earlier study for unfolding photon spectra and incident electron energies from transmission data is accurate and practical for clinical use. © *2012 American Association of Physicists in Medicine*. [http://dx.doi.org/10.1118/1.4754301]

Key words: transmission measurements, spectral unfolding, bremsstrahlung reconstruction, inverse problems, photon beams, photonuclear, `EGSnrc`

I. INTRODUCTION

For megavoltage photon beams from linear accelerators (linacs), transmission analysis is one of several methods that have been used to determine the photon spectra and/or the electron source energy. Other prominent methods include direct spectroscopy,[1,2] Compton spectroscopy,[3] spectral unfolding from depth-dose measurements,[4,5] and Monte Carlo simulation of treatment heads.[6] Compared with other methods, transmission analysis combines the advantage of clinical viability with the potential for accuracy and sensitivity to slight energy changes, as demonstrated below.

In a recent computational study,[7] an improved physics-based approach was proposed for unfolding linac photon spectra and incident electron energies from transmission data. In this approach, energy differentiation is significantly improved when the unfolding algorithm is simultaneously fed with the data of four separate transmission curves measured for low-Z and high-Z attenuators using two detectors of different energy response. The specific two detector

configurations proposed are a single Farmer chamber with two different buildup cap materials, a low-Z one and high-Z one. The photon spectrum is specified using a functional form[8] with four free parameters, one of which is the incident electron energy. The function fits a diverse set of high-precision Monte Carlo-calculated linac spectra with a RMS energy fluence deviation of 1.7%, and fits the maximum photon energies of those spectra within 1.4% of their true values. Compared with the full iterative unfolding methods, the use of a reasonably parameterized spectral functional form significantly improves the unfolding robustness, especially if the end point energy of the spectrum is treated as an unknown. The weak energy dependence of the photon attenuation coefficients at megavoltage energies makes the spectral unfolding problem very sensitive to both random and systematic sources of uncertainties. Therefore, part of the proposed approach is to account for the detector energy response, nonideal attenuation conditions, and the contribution of photonuclear attenuation for higher MV beams. The current study validates this approach experimentally and demonstrates its application on a typical clinical linac.

The spectra of clinical photon beams are typically not known independently, therefore most previous experimental studies that unfolded clinical spectra from transmission measurements resorted to indirect validation approaches. In these approaches, comparisons were made between measured spectrum-averaged dosimetric quantities and the calculations of the same quantities using the unfolded spectra. Such quantities include transmission curves, PDDs,[9–12] ratios of TPR and TMR,[9,13,14] stopping power ratios,[10,13,15,16] mass energy absorption coefficient ratios,[10] and contrast in portal images.[17] These indirect validation approaches do not reveal errors in the spectral shapes, and they are not generally sensitive to slight spectral changes. In a limited number of previous studies,[14,18–20] the unfolded spectra were visually compared with generic spectra from other studies.

In the current study, the photon spectra are unfolded from the transmission data that were recently measured[21] on the Vickers research linac of the National Research Council (NRC) Canada for a variety of MV beams and bremsstrahlung targets. The measured signals were compared to their respective `EGSnrc` (Refs. 22 and 23) calculations. A supplemental web report[24] provides tabulated data of the measured and calculated transmission values, as well as a detailed description of the experimental setup for others to benchmark Monte Carlo codes.

The photon spectra of the NRC Vickers research linac were previously measured using a NaI detector,[1,2] and the incident electron parameters are independently known: the mean energy and the energy spread are known from a calibrated bending magnet and slit system,[25] while the focal spot size and shape as well as the angular divergence are known from radiochromic film measurements.[26] The unfolded spectra in the current study are validated against the spectra measured using the NaI detector, and against `EGSnrc` spectra calculated using the known electron beams and geometric setups, with no free parameters. Therefore, the validation in this study is direct, and against spectra that are independent of the transmission measurements. The MV range of the research linac beams used in this study (10–30 MV) provides a particularly rigorous validation because the energy dependence of the photon attenuation coefficients is weakest for those beams (compared with lower MV beams), and hence accurate spectral unfolding is most challenging. Once the approach is validated on the special research linac, its use is demonstrated on a typical clinical linac (an Elekta *Precise*) for 6, 10, and 25 MV beams.

In most previous studies where photon spectra were unfolded from measured (rather than computational) transmission data, the robustness of the minimization necessitated that the maximum photon energy, E_m, be fixed to an assumed value. However, for a typical clinical linac E_m is not known, and fixing it to an assumed value can be a gross approximation. Baker and Peck[9] determined E_m by restricting their three-parameter spectral model to only one parameter to unfold E_m, then fixed E_m at that value during the full minimization. A unique aspect of the current study is that the electron energy is treated as a truly free parameter, and searched for concurrently with the other free parameters. This is made possible by the improvements in robustness and in energy differentiation.

For the rest of this paper, it is assumed that the reader is familiar with the contents of Ref. 7 for the proposed approach, and Ref. 21 for the experimental transmission measurements on the Vickers research linac.

II. MATERIALS AND METHODS

II.A. Research linac: Previous transmission measurements

Transmission signals were measured on the NRC research linac for 8 beams in the range 10–30 MV using thick Be, Al, and Pb bremsstrahlung targets. The specific MV/bremsstrahlung target combinations included are: 10/Al, 15/Be, 15/Al, 15/Pb, 15.7/Pb, 20/Al, 20/Pb and 30/Al. The smallest transmission signals are ~1.7% of those without an attenuator. For each beam, data were acquired for C and Pb attenuators using an Exradin A19 Farmer chamber with a buildup cap made of either polymethylmethacrylate (PMMA) or a W-alloy. Two of the eight beams were for 15.00 and 15.70 MeV electrons incident on a Pb target. The data for these two beams are used in the current study to demonstrate the ability of the approach to resolve small changes in the incident electron energy. Several of the sets measured with the PMMA cap were repeated with an Al cap, and a few of the sets measured with the A19 chamber were repeated with a PTW30013 Farmer chamber. These data are used in the current study to establish the detector-independence of the unfolded spectra.

Experimental corrections were applied to account for the following effects (the values in parentheses represent the largest corrections applied): drifts in the direction of the beam (2%), polarity (2.5% typical maximum, 6% extreme), ion recombination (0.2%), leakage (0.3%), and room scatter (0.8%). The largest effect was the polarity

correction for the smallest transmission signals. It is thought to be largely due to extra-cameral signals, which make a larger fraction of the smaller signals.

An experimental uncertainty budget for the measured transmission signals was constructed (Table II in Ref. 21). The uncertainty contributions associated with the following components were included: (a) linac parameters: incident electron beam parameters, correction for short-term drifts in the beam direction, and, long-term stability of the energy of the electron beam; (b) detection systems: polarity, ion recombination, leakage, monitor chamber stability, and electrometer nonlinearity; (c) attenuators: inexact mass thickness, density nonuniformity, and impurities; and (d) setup parameters: misalignment and positioning uncertainties. The uncertainty varies with beam energy and with attenuator material, and it increases as the transmission signal decreases. A representative uncertainty on the smallest transmission signals is 0.42% and 0.65% without and with the uncertainties on the incident electron parameters, respectively. In the current study, the uncertainties on the transmission signals are used during the minimization (Sec. II.F) to extract the confidence bounds on the unfolded spectra and the unfolded incident electron energies.

II.B. Research linac: Direct independent validation methods

This section presents some considerations to facilitate the validation of the unfolded spectra for the research linac beams against the NaI-measured spectra and their corresponding EGSnrc spectra. The differences between the transmission measurement setup[21] and the NaI measurement setup[1,2,27] are listed in Table I. The uncertainties on the geometry and electron parameters listed in the table are discussed in the original publications of the two experiments. While there are differences in the pretarget materials, there are no post-target differences listed because such differences (e.g., collimator effects) are explicitly corrected for in both experiments. Many of the differences listed for the electron parameters are due to the introduction of a the slit system whose function is discussed below.

The first difference shown in Table I is the dose rate, which can affect the incident electron beam, and consequently the resulting bremsstrahlung spectra. However, in the Vickers linac used in this study, the electron beam characteristics at the exit window are controlled by the settings of the combined magnet/slit system at the end of a very long drift tube. Therefore, changes in the dose rate are unlikely to change the spectrum, and it is thus justified to benchmark the spectra unfolded from transmission data measured at near-therapeutic dose rates against the NaI spectra measured at ultralow dose rates.

The remaining differences between the two experiments lead to small differences in the spectra. To investigate this and account for it, the energy fluence spectra at the detector location in both setups are generated using EGSnrc. In these simulations, post-target components are not included since their effects are corrected for. The KM option is used for more accurate[21,27] bremsstrahlung angular sampling. The NRC option for bremsstrahlung cross sections is used (which is the NIST cross sections except that the electron-electron bremsstrahlung component is replaced with a more accurate model[28]). The newly added option to model photonuclear attenuation[29] is included. The photon energy cutoff is 10 keV. The NaI setup details are taken from Ref. 27, and the transmission setup details for the case with no attenuator are taken from Ref. 24. For each setup, the energy fluence spectra are extracted at the detector location in a scoring circle of the size of the collimated beam. The statistical uncertainty on the EGSnrc spectra are made negligible compared to the investigated spectral differences. Results show that the dominant contributor to the spectral differences between the two experiments is the difference in the pretarget materials. The RMS energy fluence deviation between the energy fluence spectra of the two setups is of the order of a few percent. The beam with the largest RMS deviation (5%) is that with the Be

TABLE I. For the research linac, a list of the differences between the transmission measurement setup (Ref. 21) and the NaI measurement setup (Refs. 1, 2, and 27).

Aspect of difference	NaI setup	Transmission setup
Dose rate at ~3 m	~1 photon/pulse	~40 cGy/min
Pretarget material	0.013 cm pure Ti exit window + 0.01(5)[a] cm pure Si monitor + 0.0051 cm steel chamber wall + 1.685 cm air	0.00412 cm Ti alloy exit window, 4.42 g/cm^3, (90% Ti, 6% Al, 4% V) + 2.05 cm air
Three target thicknesses		
(a) Pb for 10, 20 MV	0.805, 1.008 cm	0.793, 1.016 cm
(b) Al for 30 MV	6.00 cm	6.60 cm
Photon beam cone half angle	0.22°	0.29°
Incident electron beam parameters		
(a) Two mean energies	15.18, 30.45 MeV	15.00, 30.00 MeV
(b) Energy spread	Gaussian, $\sigma = 0.64\%$	Gaussian, $\sigma = 0.4\%$
(c) Radial spread	Uniform circle, dia. 0.35 cm	Gaussian, 1 mm FWHM
(d) Angular divergence	Assumed none in Ref. 27	0.03°, apex 1 m upstream of exit window

[a]It is 0.010 cm for the Be target and 0.015 cm for the Al and Pb targets.

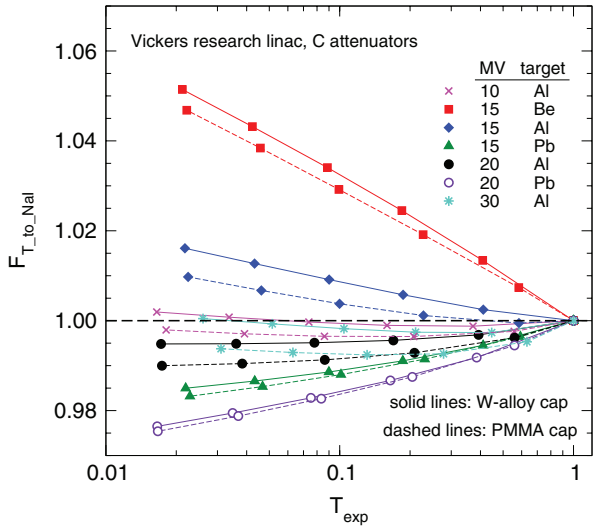

FIG. 1. For the research linac, the "transfer" factor $F_{\text{T-to-NaI}}$ versus the experimental transmission, T_{exp}, for C attenuators. The corresponding transfer factors for Pb attenuators are much smaller ($\leq$1.6% from unity).

target. This is because, compared with other targets, the disparity is largest between the atomic number of Be and the effective atomic number of the pretarget materials.

A "transfer" factor, $F_{\text{T-to-NaI}}$, is used to account for the differences between the two experiments. Multiplying the experimental transmission signals by $F_{\text{T-to-NaI}}$ before the unfolding enables the comparison between the unfolded spectra and their respective NaI-measured ones. The factor $F_{\text{T-to-NaI}}$ is called a "transfer," rather than a "correction," factor because it is specific to this primary benchmark study which compares two experiments, and it is not needed for any clinical measurement setup. For a given attenuator material and mass thickness, $F_{\text{T-to-NaI}}$ is defined as the transmission value using the energy fluence spectrum with the NaI setup parameters in Table I divided by the corresponding transmission value using the spectrum with the transmission setup parameters. Each of the two transmission values is calculated using

$$T = \frac{\int_{E_l}^{E_m} R(E)\psi(E)\exp\left(-\mu(E)x_i\right)dE}{\int_{E_l}^{E_m} R(E)\psi(E)dE}, \quad (1)$$

where T is the transmission value, $\psi(E)$ is the photon energy fluence at energy E, $R(E)$ is the detector energy response per unit energy fluence at E (precalculated[7] using `EGSnrc`), x_i is the attenuator mass thickness, $\mu(E)$ is the mass attenuation coefficient of the attenuator material at E, and E_l and E_m are the lowest and maximum photon energy, respectively. Figure 1 shows the variation of $F_{\text{T-to-NaI}}$ with transmission. The transfer factor is generally small ($\leq$2.5% from unity), except for the beam with the Be target (up to 5.1% from unity) because of the pretarget material differences discussed above.

II.C. Clinical linac demonstration: Transmission measurements

Transmission measurements are performed on-axis on an Elekta *Precise* linac for 6, 10, and 25 MV beams. The three beams use the same bremsstrahlung target but different flattening filters. The details of the apparatus and measurement protocol are the same as those discussed previously in detail for the research linac,[21] except for the specifics below.

The first stage of collimation is achieved using the linac internal jaws to create a 3 × 3 $(\text{cm})^2$ field at 100 cm. A second Pb collimator of 10.2-cm thickness and a nondiverging 0.77-cm-diameter opening is mounted on a custom "shadow tray" at 60 cm from the upstream surface of the bremsstrahlung target. The tray is made of Al for rigidity and has an opening diameter much larger than the collimated beam. An inhouse external monitor chamber is mounted between the jaws and the second collimator. The chamber consists of two outer layers of aluminized Mylar, 6 μm-thick each, and two electrodes of gold-plated Kapton, 125 μm-thick each. Its sensitive volume is a central cylinder of diameter 11.5 cm and thickness 2 mm. The chamber is used for output normalization instead of the built-in multielement chamber of the linac to avoid potential uncertainties from the complex feedback mechanisms of the latter. Unlike the measurements on the research linac, the small field created by the jaws precludes the use of a field chamber between the two collimators to monitor drifts in the beam direction.

A computer-controlled linear translation system is used for the attenuator sets. The upstream surface of the attenuators is placed at the plane of the machine isocenter at 100 cm. Ten lengths are used per attenuator material (five for each detector). For the 6, 10, and 25 MV beams, respectively, the maximum attenuator lengths are 64, 83, and 116 cm for C, and 7.5, 7.5, and 7.0 cm for Pb. The corresponding smallest transmission values are ~2%. For the 6 MV beam, additional measurements are performed with Cu attenuators (maximum length 11 cm). The Cu data are used to test the attenuator-independence of the unfolded spectra by comparing the spectra unfolded using C + Cu data against those using C + Pb data. For all MV beams, a short Cu rod is permanently fixed in the attenuator assembly, with its upstream surface placed on the same plane as the attenuator set. Similar to the research linac measurement, the "Cu-to-monitor" ratio is used to correct for possible drifts in the beam direction. A third Pb collimator is placed past the attenuator assembly at 291 cm. It is 15.3-cm thick, with a nondiverging opening diameter of 2.9 cm. Each of the Pb-collimation stages are aligned to the light field using two orthogonal telescopes. The overall alignment relative to the beam central axis is within 1 mm at 3 m.

Transmission signals are acquired at ~310 cm using an Exradin A19 Farmer chamber, once with the PMMA cap and once with the W-alloy cap. To reduce the magnitude and uncertainties of leakage and polarity effects, the Farmer chamber is connected with a short cable to a Keithley 6517A electrometer which is placed inside the linac room and lightly shielded. Compared with the soft flattening-filter-free beams of the research linac, the clinical beams have flatter profiles at the Farmer chamber location, which reduces the effect of chamber positioning uncertainties. Measurements are performed using a horizontal beam position to reduce floor backscatter into the chamber and cables. The nearest wall to the Farmer

chamber is ~2 m away, with negligible backscatter contribution.

The measured Farmer chamber currents with the W-alloy cap and with no attenuator present are ~150 to 250 pA going from 6 to 25 MV. These currents correspond to a dose rate to water of ~45–75 cGy/min if the bare chamber were in a water phantom. With the longest attenuators, the Farmer chamber currents are ~50 times lower. Unlike the research linac, which has minimal feedback, the continuous feedback in the clinical linac causes larger fluctuations in the signals that were acquired with short charge collection time (5 s for the signals with no attenuators). For these signals, in order to maintain a 0.1% standard deviation on the mean for short-term repeatability, the number of repeat measurements is increased threefold compared to the research linac measurements.

The correction for output fluctuations using the external monitor chamber signal is ≤1%, and the correction for short-term drifts in the beam direction using the "Cu-to-monitor" ratio is ≤0.25%. These corrections are smaller than their respective ones for the research linac beams (≤3.5% and ≤2%) because the continuous feedback mechanisms in the clinical linac lead to a more stable output.

Figure 2 shows the measured polarity correction, P_{pol}, defined as in the AAPM TG51 protocol,[30] with the negative signal as the reference. Similar to P_{pol} for the research linac beams (Sec. II.A), it is the largest experimental correction and can be up to 6% for the smallest signals in the highest MV beam (the corresponding difference in the currents with either polarity is only a few hundred fA). The larger P_{pol} values for the 25 MV beam can be explained by the larger scatter into the chamber cables. This is due to a combination of increased head leakage, increased leakage through the collimators, and larger penetrating fraction of the beam through the detector, all of which lead to more radiation in the room. The value of P_{pol} is larger with the PMMA cap, which could be caused by the smaller signal with the PMMA cap and/or by more scatter from the cap into the cables. The value of P_{pol} is marginally larger for C attenuators compared with Pb. Despite the relatively large P_{pol}, the polarity-corrected signals are found to be consistent within repeatability uncertainties. This suggests that the assumption that the causes of polarity cancel out when averaging the absolute signals of the two opposite polarities is valid. The ion recombination and room scatter corrections are found to be very similar to those for the research linac beams.

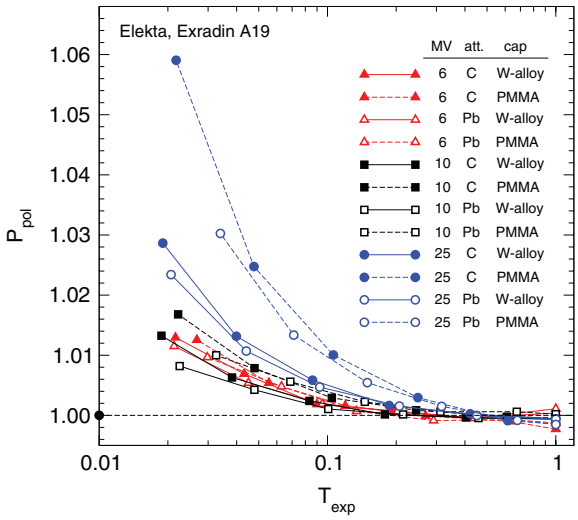

FIG. 2. For the clinical linac, the polarity correction factor, P_{pol}, versus the experimental transmission signals, T_{exp}, for different beams, attenuators and buildup caps.

The experimental uncertainty budget on the measured transmission signals is derived according to The ISO Guide on Uncertainty in Measurement,[31] similar to that done previously for the research linac beams (Table II in Ref. 21). The two main differences for the clinical beams are: (a) the uncertainty component due to short-term repeatability is smaller, and (b) the uncertainties on the incident electron parameters are ignored because these parameters are typically unknown, and because the clinical linac is not used as the primary benchmark. The typical standard uncertainty on the smallest transmission (not including electron beam uncertainties) is 0.35%.

II.D. Clinical linac demonstration: Validation methods

Unlike the research beams, direct independent validation is not available for the clinical beams. Therefore, the unfolded quantities are validated using the two methods described below. The two methods combined constitute a rigorous test of the unfolding accuracy.

The first method validates the unfolded electron energy only, and does not involve using the unfolded spectral shape. In this method, `EGSnrc` is used to calculate transmission values from a full model of the experimental setup, and these data are compared to the measured transmission signals. The incident electron energies used in the `EGSnrc` simulations are the unfolded values from the transmission measurements (Sec. III.B). The other needed electron parameters are taken from Tonkopi *et al.*,[32] where they were estimated using in-air off-axis ratio measurements on the same linac. Those other parameters are: (a) energy spread: none, (b) focal spot: Gaussian with FWHM values of 0.15, 0.05, and 0.19 cm for the 6, 10, and 25 MV beams, respectively, and (c) mean angular divergence: none for the 6 and 10 MV beams and 1.15° for the 25 MV beam. The linac head and the detector are modeled using proprietary information from their respective manufacturers. `BEAMnrc` (Refs. 33 and 34) is used to model the linac head and the transmission setup, then used as a shared library input to the usercode `cavity`[35] which models the detector. The newly added option in `EGSnrc` for photonuclear attenuation[29] is included everywhere except in the detector. Its effect at 25 MV on the smallest calculated transmission values is 1.5% for C attenuators and 2% for Pb, and its effect is negligible for the 6 and 10 MV beams.

The second method validates the spectral shape only. In this method, the unfolded spectra are compared with those from `BEAMnrc` simulations of the transmission measurement setup without an attenuator. The simulations use the unfolded incident electron energies, in combination with the other electron parameters from Ref. 32. Energy fluence

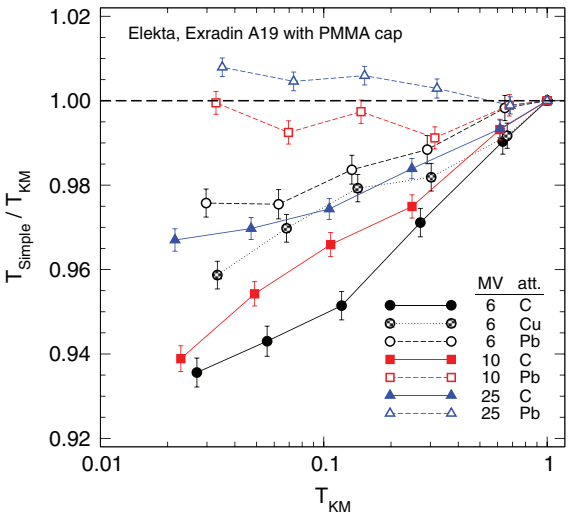

FIG. 3. For the clinical linac, the effect of using the different bremsstrahlung angular sampling options offered in EGSnrc on the calculated transmission, T.

spectra are extracted from phase space files at the attenuator surface in a scoring circle of the size of the collimated beam. The extracted spectra do not include collimator scatter contribution for consistency with the unfolded spectra since the collimator effects are corrected for during the unfolding (Secs. II.E and II.F). In this validation method, by definition, the EGSnrc spectra and the unfolded spectra have an identical endpoint energy; therefore, this method validates only the unfolded spectral shapes, as a complement to the first method.

In all EGnrc simulations for the clinical linac, the KM option is used for more accurate[21,27] bremsstrahlung angular sampling. However, it is found to be six times less efficient than the other EGSnrc angular sampling option, Simple, when the directional bremsstrahlung splitting variance reduction technique[36] is used. In light of this large efficiency difference, it is useful to note the difference in the calculated transmission values using the two sampling options. Figure 3 shows that the differences are as large as 6.4%. The differences increase with decreasing MV (3.3% to 6.4% going from 25 to 6 MV for C attenuators) because the incident electrons scatter more, which makes on-axis signals more sensitive to the angular distribution details. For the 6 MV beam, the effect increases with decreasing atomic number of the attenuator (2.4% to 6.4% going from Pb to C) because of the difference in the attenuator sensitivity to spectral changes.[21]

II.E. Role of Monte Carlo during the unfolding

In this study, the role of Monte Carlo in spectral unfolding is in two areas: detector energy response modeling and corrections for certain nonideal attenuation conditions.

For the detector energy response, the main detector is the Exradin A19 chamber fitted with the PMMA or W-alloy caps. A third Al cap, as well as a PTW30013 chamber, were used for some of the research linac measurements, as discussed in Sec. II.A. The detector energy response per unit energy fluence [$R(E)$ in Eq. (1)] was previously[7,21] calculated using EGSnrc and validated experimentally.

The Monte Carlo correction for nonideal attenuation accounts for the deviations that are difficult to eliminate or correct for experimentally. In the transmission measurement setup of this study, these deviations include: (a) forward scatter (coherent or incoherent) and positron annihilation events in the irradiated attenuator, (b) collimator effects caused by interactions within the collimators or by leakage of the primary radiation through their edges, (c) attenuation and scatter by the intervening air, (d) possible electron contamination in the highest MV beam where the caps do not provide full buildup, and (e) backscatter from the linac room wall. Two Monte Carlo-based methods were previously proposed[7] to correct for these (and similar) deviations during spectral unfolding: an iterative method and a system response matrix method. The two methods were validated using computational transmission data generated using known spectra. In this study, the iterative method is used to estimate a correction factor, F_{nonideal}, to the measured transmission signals which accounts for the combined effect of the deviations listed above. The use of this method during the unfolding is described in Sec. II.F.

Given that the detector energy response is experimentally validated, and that the correction for nonideal attenuation is not very sensitive to the spectrum used to estimate it, it can be said that there is no significant Monte Carlo bias during the unfolding, and thus the results can still be considered "independent experimental" spectra.

II.F. Unfolding details

For a given MV beam, the data of the four measured transmission curves from the different attenuator/cap combinations are fed simultaneously to the unfolding algorithm. For the research linac beams, the experimental transmission signals are multiplied by the transfer factor $F_{\text{T-to-NaI}}$ before being used as input. During the minimization, each experimental transmission data point is weighted by the inverse of its variance. The variance is determined from the total experimental uncertainty on that point (Sec. II.A), including the uncertainties on the incident electron parameters and other systematic uncertainties. These uncertainties are propagated into the confidence bounds on the unfolded quantities using the methods of Ref. 37. For the clinical linac beams, the details above apply, except that $F_{\text{T-to-NaI}}$ is not required, and the variances used for weighting the input transmission data do not include the uncertainties on the incident electron parameters, which are unknown in this case.

The energy fluence spectrum is unfolded using Levenberg-Marquardt least-squares minimization.[38] The spectrum is specified using a validated four-parameter functional form.[8] The incident electron energy is one of the four free parameters, and it is searched for concurrently with the other three (an exception is the 30 MV beam of the research linac, where robust minimization necessitates doing an exhaustive (grid) search on the electron energy while minimizing the objective function with respect to the other three parameters). The

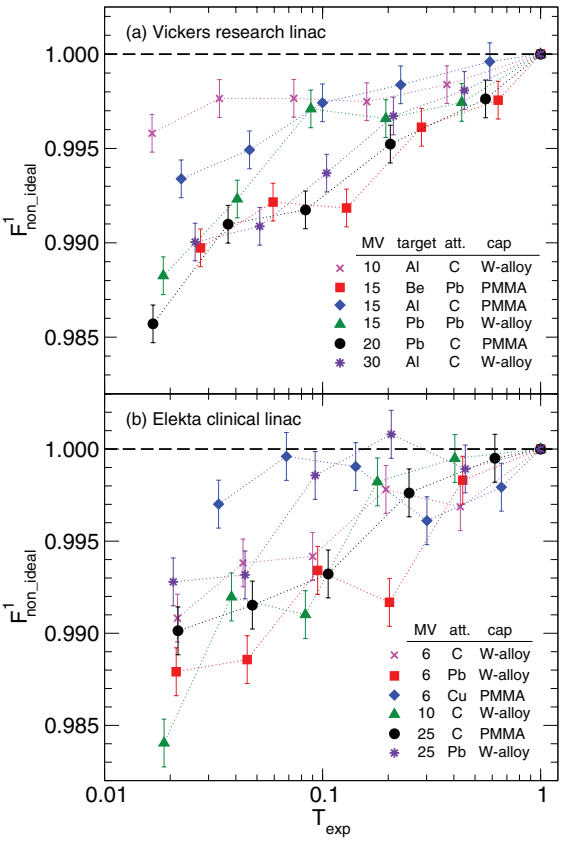

FIG. 4. The correction factor F^1_{nonideal} versus the experimental transmission, T_{exp}, after one iteration (hence the superscript 1).

minimized objective function is χ^2, the sum of the squares of the inverse-variance-weighted difference between the input transmission signals and the values calculated from Eq. (1) using the estimates of the four free parameters in a given iteration. The photon cross sections used during the unfolding [$\mu(E)$ in Eq. (1)] are the NIST XCOM compilation[39] plus the IAEA photonuclear data.[40] The effect of photonuclear attenuation on the calculated transmission values in Eq. (1) is $\leq$5.2% for the higher MV beams of the research linac, and $\leq$2% for the 25 MV beam of the clinical linac; the effect decreases for lower MV beams. The uncertainties in $\mu(E)$ are not included in the estimate of the confidence bounds on the unfolded quantities. Numerical uncertainties from the integration and from the interpolations in the detector energy response and in the photon cross sections are made negligible. The minimization is robust against different initial estimates of the free parameters, including the electron energy (within many MeV of the nominal MV of the beam). No *a priori* knowledge of the linac head details is required. Minimization takes very few seconds.

To implement the correction for nonideal attenuation conditions, the unfolded spectrum is used as a point source in `EGSnrc` simulations of the transmission setup to estimate the factor F_{nonideal} (introduced in Sec. II.E). In these simulations, the point source is placed roughly at the location of the bremsstrahlung target to replace the whole linac head. Our `EGSnrc` sensitivity analysis shows that the correction factor is not sensitive to the exact location of the point source (within many centimeters). Therefore, the only knowledge required of the linac head in the calculations to estimate F_{nonideal} is a crude estimate of the target location. Figure 4 shows examples of the estimated F_{nonideal}. The magnitude of the correction is determined by the interplay of many factors, and it can be as large as 1.5% of the smallest transmission signals. The estimated F_{nonideal} is used to computationally correct the input transmission signals, and a revised spectrum is unfolded. In practice, only one iteration is needed for the spectrum to converge. Smooth quadratic fits of F_{nonideal} values as a function of transmission signal (e.g., those in Fig. 4) are applied to the experimental data before unfolding the final spectrum. The quadratic fits are well-within the uncertainties on the correction (typically 0.1%).

With 16 degrees of freedom (20 measurement points minus four free parameters), the typical final reduced χ^2_{min} is lower than unity. Given that the spectral functional form is not overparameterized, a lower than-unity χ^2_{min} implies that the experimental uncertainty budget is conservative—possibly from ignoring the correlation between the uncertainty components, and/or from using extreme effects to deduce some components.

III. RESULTS AND DISCUSSION

III.A. Research linac unfolded data

For the research linac beams, comparisons of the unfolded spectra and the unfolded incident electron energies, E_e, against the benchmark data are shown in Fig. 5 and Table II.

The spectra in Fig. 5 and the RMS energy fluence deviations in Table II are based on normalization of each spectrum to unit energy fluence. This method of normalization gives more reasonable weight to the higher energy portion of the spectrum compared with normalization to unit fluence, and graphically reveals the discrepancies better. It also avoids the potential bias from normalization to a specific point (e.g., the peak).

The 95% confidence bounds in Fig. 5 are determined by the variances used for weighting the input transmission signals during the minimization. The bounds include the effect of the uncertainties in the incident electron parameters, and the effect of other experimental systematic uncertainties. However, the bounds do not include the effect of cross section uncertainties or the systematic errors from the functional form. The bounds are generally tight, which is a direct result of the small experimental uncertainties. For the unfolded 30 MV spectrum, the bounds are larger because the incident electron energy is obtained through a grid search, where the correlation between the electron energy and the other free parameters is missing, which is found empirically to lead to more conservative uncertainty bounds. The bounds have an irregular shape, typically with two necks. This is a result of conforming the spectral shape to the functional form, where some energy fluence values are more likely to be crossed by the unfolded spectrum than others. This shape was previously validated[8] using

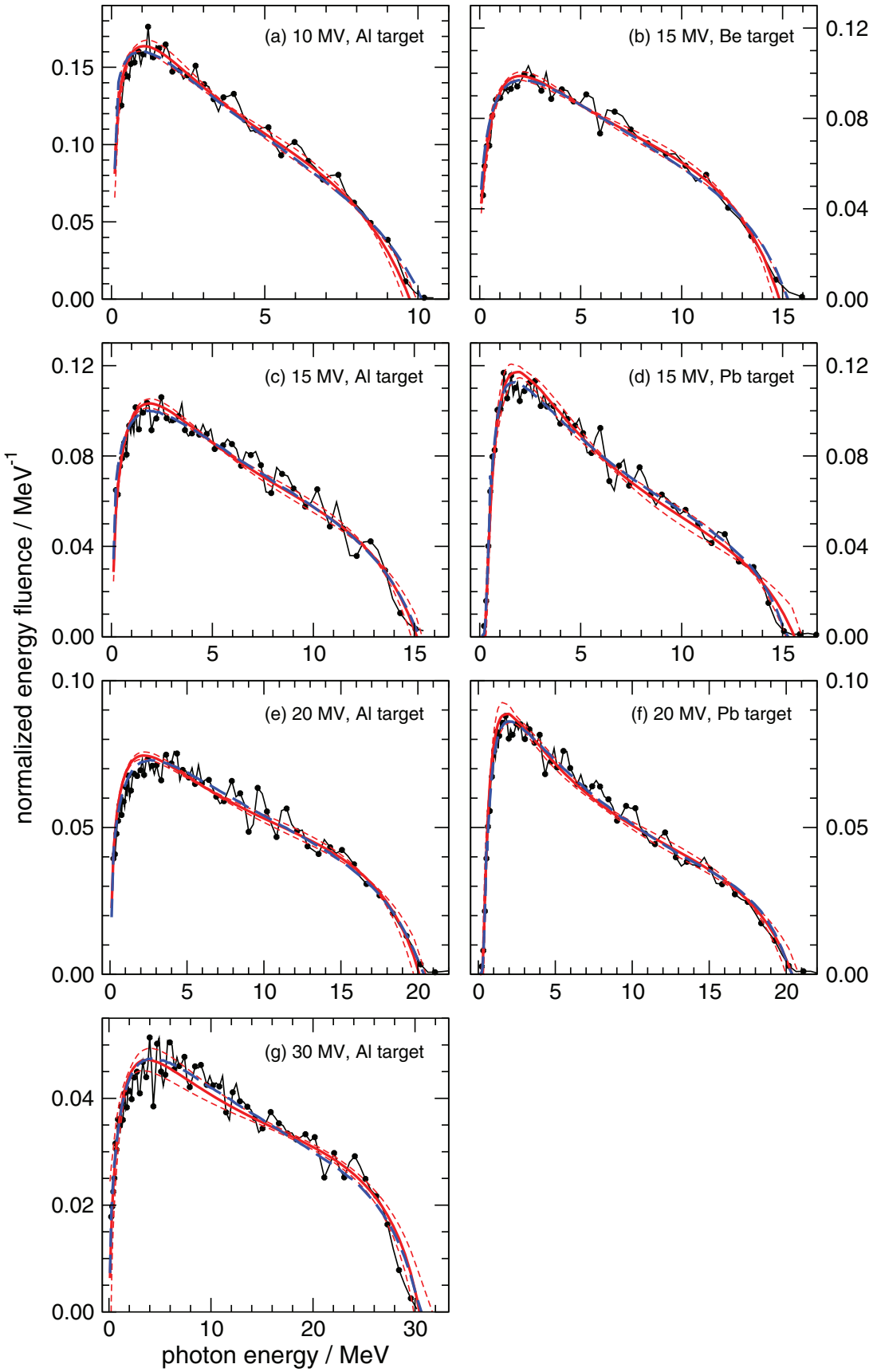

FIG. 5. For the research linac beams, comparison of the spectra unfolded from transmission measurements against the benchmark NaI-measured spectra (Refs. 1 and 2) and their corresponding EGSnrc spectra. The NaI-measured spectra are the thin solid lines with every other data point shown as a small circle. The EGSnrc spectra are the thick long-dashed lines, with negligible statistical uncertainty. The unfolded spectra are the thick solid lines, with the 95% confidence bounds shown as two thin short-dashed lines. Spectra are normalized to unit energy fluence.

TABLE II. For the research linac beams, evaluation of the accuracy of the unfolded energy-fluence spectra, ψ, and the unfolded incident electron energies, E_e. For the differences between the unfolded and the EGSnrc spectra, $\Delta\psi$ is the RMS energy fluence deviation (normalized to the mean energy fluence), and ΔE_{mean} is the difference in the mean energy. ΔE_e is the relative difference in E_e between the unfolded and the bending magnet values. The bending magnet values are those used during the NaI measurements (Refs. 1, 2, and 27) (Sec. II.B).

MV	Brem. target	$\Delta\psi$ (%)	ΔE_{mean} (MeV)	E_e (magnet) ± 1 s.d. (both in MeV)	E_e (unfolded) ± 1 s.d. (both in MeV)	ΔE_e (%)
10	Al	4.5	0.02	10.09 ± 0.04	9.73 ± 0.11	− 3.5
15	Be	4.8	0.09	15.18 ± 0.06	14.84 ± 0.19	− 2.3
	Al	4.8	0.10		15.13 ± 0.13	− 0.3
	Pb	5.5	0.02		15.59 ± 0.19	2.7
20	Al	4.0	− 0.11	20.28 ± 0.08	20.10 ± 0.21	− 0.9
	Pb	5.1	− 0.11		20.38 ± 0.22	0.5
30	Al	3.1	0.12	30.45 ± 0.12	30.44 ± 0.63	0.0

analytical transmission data smeared with simulated experimental noise.

The accuracy of the unfolded spectra is discussed here. The 95% confidence bounds on the unfolded spectra mostly fall within the statistical noise of the NaI data. The comparison of the unfolded spectra against the high precision EGSnrc spectra also show good agreement, with some small differences. The RMS energy fluence deviation is typically 4.5% (the average of the data in the third column of Table II), and the deviations in the mean spectrum energy are less than 150 keV. There are several reasons that contribute to the differences between the EGSnrc and the unfolded spectra beyond the confidence bounds. (a) Different normalization methods lead to different positioning of the spectra relative to each other and hence the regions of discrepancy could change. (b) Systematic errors from conforming the spectral shape to a four-parameter functional form, which are not part of the confidence bounds shown—N.B., when the function is fit directly to a variety of high-precision spectra, there is a 1.7% RMS energy fluence deviation.[8] (c) Uncertainties in the photon cross sections that are used during the unfolding [$\mu(E)$ in Eq. (1)]. (d) The accuracy of the benchmark EGSnrc spectra, which are affected by second-order limitations in the underlying physics models (e.g., the bremsstrahlung energy-angle relations)—an indication of this possibility is that the spectra generated by different mature Monte Carlo codes show some differences.[27]

From Table II, the comparison of the unfolded E_e values against their respective bending magnet values show that the accuracy of unfolding the incident electron energy is ∼3%. For the measurements from Sec. II.A with electron beams of energies 15.00 and 15.70 MeV (a 4.7% energy change) incident on a Pb target, the unfolded electron energies are, respectively, 15.4 ± 0.2 MeV (1 s.d.) and 16.3 ± 0.2 MeV (1 s.d.). The unfolded values are within ∼3% of their true values, and they are outside the 95% confidence bounds of each other. This confirms the ∼3% resolving power of the technique.

To test the independence of the unfolded spectra from the detector, the input transmission data for the PMMA cap are replaced with those for the Al cap (in combination with the W-alloy cap data in both cases), and the corresponding detector energy response is used during the unfolding. Strong overlap is observed between the confidence bounds of the spectra unfolded using the two data sets. The RMS energy fluence deviation between any two of such unfolded spectra are smaller than the overall accuracy of the technique (viz., the 4.5% average value from Table II). The same results are obtained when the data for the Exradin A19 are replaced with those for the PTW30013 chamber (with its corresponding energy response used during the unfolding). These results indicate that the unfolded spectra do not have systematic detector-related bias.

Figure 6 illustrates the effect of different variations of the input data on the unfolding accuracy. From Table II, the RMS energy fluence deviation, $\Delta\psi$, for the 20 MV beam from a Pb target is 5.1%. When only one attenuator that has a monotonic attenuation coefficient (i.e., C), and one detector (A19 with a W-alloy cap) are used (which is the approach used in

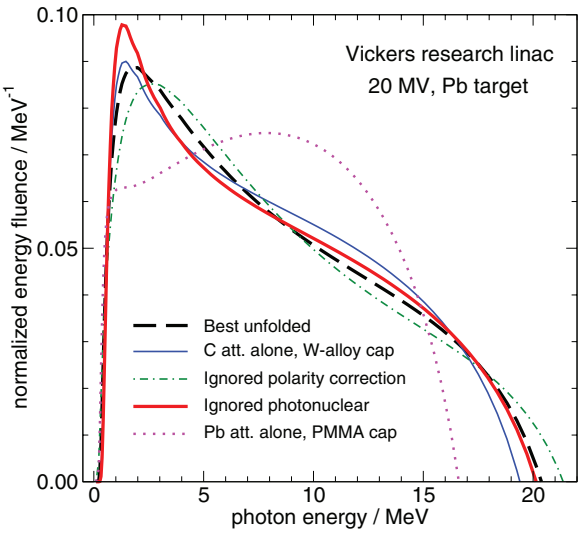

FIG. 6. For the research linac, investigation of the effects on the accuracy of the unfolded spectra when using different variations of the input transmission data and when ignoring different influence quantities. "Best unfolded" is the unfolded spectrum from Fig. 5(f). The other four curves are the unfolded spectra for the situations shown in the legend. Spectra are normalized to unit energy fluence.

previous studies), $\Delta\psi$ worsens to 11.2%, even with the high accuracy of the transmission measurements. When the polarity correction is ignored, $\Delta\psi$ worsens from 5.1% to 8.9%. When the photonuclear effect is ignored, $\Delta\psi$ worsens from 5.1% to 14.9%. The examples in Fig. 6 underline the importance of the various computational and experimental effects investigated. As a theoretical exercise, if Pb is the only attenuator used, the unfolding becomes degenerate by definition (because the attenuation coefficient for Pb is not monotonic in the energy range of interest), and wrong spectra are likely, as seen in Fig. 6.

III.B. Clinical linac unfolded data

For the Elekta *Precise* beams, the unfolded quantities and their validation (using the two methods discussed in Sec. II.D) are shown in Figs. 7 and 8, and in Table III. The details of the normalization and the confidence bounds are the same as those for the research linac beams (Sec. III.A), except that the confidence bounds do not account for the uncertainties on the incident electron parameters.

For the first method, which validates only the unfolded electron energy, E_e, Figs. 7(a)–7(c) show that the EGSnrc transmission data, which are calculated using the unfolded incident electron energies, agree with the measured signals within ~1.5% (three times the uncertainty on the ratios). This can be caused by several uncertainty components that are not part of the error bars in Fig. 7, including: (a) the uncertainty on the unfolded electron energy (which is affected, in part, by the systematic errors in the spectral functional form); (b) the uncertainties on the other incident electron parameters taken from Tonkopi *et al.*;[32] (c) the uncertainties in the photon cross sections used in the Monte Carlo calculations; and (d) the accuracy of the relevant physics models in EGSnrc (as noted for the research linac beams).

TABLE III. For the beams of the clinical linac (an Elekta *Precise*), comparison of the unfolded spectra against the EGSnrc spectra. The definitions of $\Delta\psi$ and ΔE_{mean} are the same as in Table II. Also shown are the estimated E_e values from other studies on the same linac.

			E_e (MeV) ± 1 s.d. (MeV)		
MV	$\Delta\psi$ (%)	ΔE_{mean} (MeV)	Unfolded, this study	From off-axis ratios (Ref. 32)	From electron depth-dose (Ref. 32)
6	2.8	0.01	6.1 ± 0.1	5.75	5.7 ± 0.4
10	4.0	−0.06	9.3 ± 0.1	9.4	9.0 ± 0.4
25	4.4	−0.33	19.3 ± 0.2	19.0	19.9 ± 0.7

Tonkopi *et al.*[32] extracted the incident electron energies for the same linac using in-air off-axis ratio measurements. They also inferred them using the combination of electron beam depth-dose data and the current settings for the linac bending magnet. Their estimates using the two methods are shown in Table III. Our unfolded E_e values differ from the off-axis ratio estimates by +6.3%, −1.2%, and +1.5% for the 6, 10, and 25 MV beams, respectively. This is investigated here for the case with the largest difference (i.e., 6 MV). We used their off-axis ratio estimate of E_e (5.75 MeV) in EGSnrc simulations of our setup to calculate the corresponding transmission values. Figure 7(d) shows that the calculated transmission values differ from the measured signals by up to 9.7%, 5.0%, and 2.7% for the C, Cu, and Pb attenuators, respectively. The corresponding differences when using the value of E_e unfolded in the current study are within 1% for all attenuators [Fig. 7(a)], which indicates that it is a more realistic estimate of E_e. This observation is supported by an unpublished extension of the recent work on the effective point of measurement.[41] In this extension, Tessier found that an E_e value of 6.0 MeV leads to better agreement than 5.75 MeV between measured and EGSnrc-calculated depth-dose curves

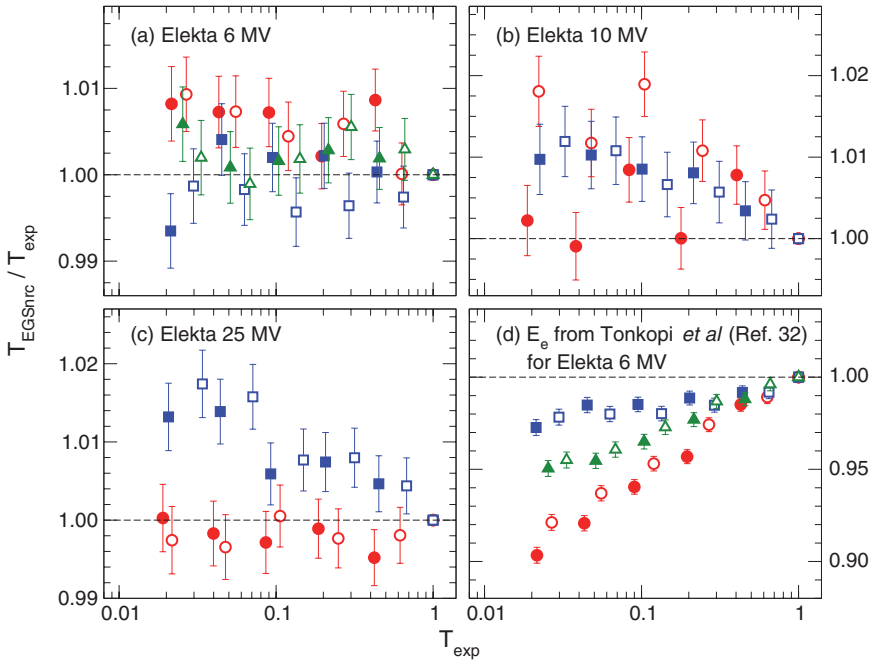

FIG. 7. For the clinical linac (an Elekta *Precise*), panels (a)–(c) show the comparison of the EGSnrc transmission values, T_{EGSnrc} (calculated using the unfolded incident electron energies, E_e), to the experimental transmission signals, T_{exp}. The data are for the following attenuator/buildup-cap combinations: C/W-alloy (●), C/PMMA (○), Pb/W-alloy (■), Pb/PMMA (□), Cu/W-alloy (▲), and Cu/PMMA (△). Panel (d) shows the same comparison as in panel (a) but when using the E_e value estimated by Tonkopi *et al.* (Ref. 32) from in-air off-axis ratio measurements on the same linac. The data equivalent to panel (d) for the 10 and 25 MV beams show significantly smaller differences (≤3.3% from unity). Note the very different scale of the ordinate of panel (d).

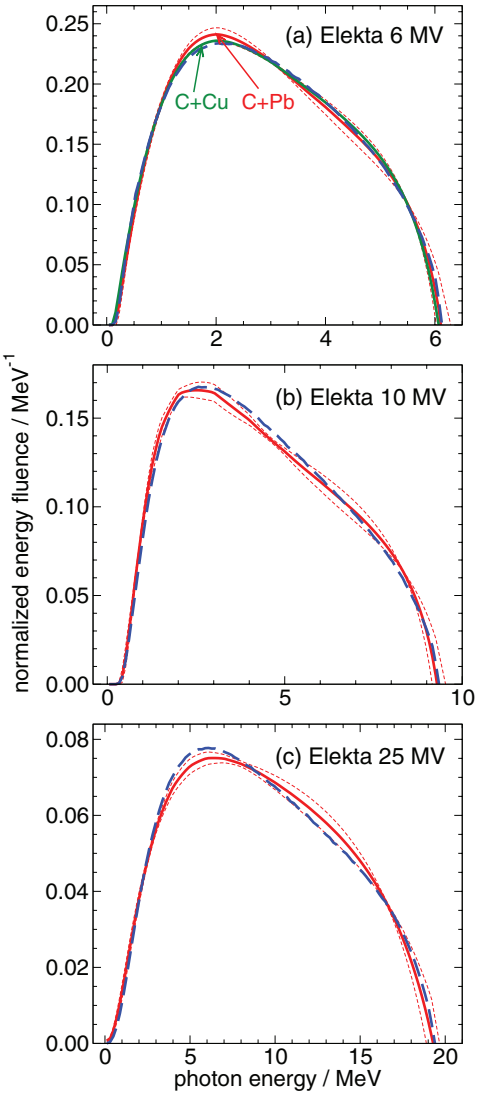

FIG. 8. For the clinical linac (an Elekta *Precise*), comparison of the spectra unfolded from measured transmission signals (thick solid lines) against the EGSnrc spectra (thick long-dashed lines) calculated using the unfolded incident electron energies. The 95% confidence bounds on the unfolded spectra are the two thin short-dashed lines. All spectra are unfolded from the combined data of C + Pb attenuators, except for an additional spectrum in panel a which is unfolded using C + Cu data. Spectra are normalized to unit energy fluence.

(including a faithful detector model).[42] The level of agreement in Figs. 7(a)–7(c) loosely suggests that the other electron parameters used in this study, which are taken from Tonkopi *et al.*,[32] are acceptable. The exercise just performed to test the effect on simulated transmission signals when using different E_e values shows strong sensitivity, which is a useful attribute of the validation method.

For the second method, which validates the spectral shape only, Fig. 8 shows good agreement between the unfolded and the EGSnrc-calculated spectra, with a typical RMS energy fluence deviation of 3.7% (the average of the data in the second column of Table III). The possible reasons for the discrepancies are the same as those discussed for the research linac beams (Sec. III.A), in addition to the uncertainties in the incident electron parameters, which are unknown for the clinical linac beams. Figure 8(a) for the 6 MV beam shows that when the data for the C + Cu attenuators are used, the unfolded spectrum is very close to that with the C + Pb data. This indicates that the unfolded spectra do not have systematic attenuators-related bias, as long as the attenuation coefficient for at least one of the attenuators is monotonic in the energy range of interest.

Overall, the combination of the two methods above constitutes a rigorous validation of the unfolded quantities for the clinical beams.

III.C. Higher transmission cutoffs

It was shown computationally[7] that when transmission data down to only 10% (as opposed to 1%–2%) are used to unfold spectra, there is only a modest reduction in accuracy ($\Delta\psi$ worsened from 2.3% to 3.2%), with some widening in the confidence bounds. In the current study, this observation is tested experimentally using the research linac data, and similar results are obtained. Using a 10% cutoff significantly reduces the magnitude and the uncertainty of many computational and experimental influence quantities. However, it reduces energy differentiation and thus increases the demand on measurement accuracy. A cutoff much higher than 10% is found to reduce the robustness, and the results become case-specific. Accurate measurements down to ~1%–2% remain useful for more energy differentiation, tighter confidence bounds, more rigorous benchmarking for Monte Carlo codes, and evaluation of photon cross section uncertainties.

IV. CONCLUSIONS

This study experimentally validates a recently proposed transmission analysis approach for unfolding the photon spectra and the incident electron energies for clinical photon beams. A unique aspect of this study is the direct independent validation on the dedicated research linac. Energy fluence spectra are unfolded with RMS energy fluence deviations of 4.5%, and the accuracy of unfolding the electron energy is ~3%. The unfolding does not require knowledge of the linac head details or *a priori* knowledge of the electron energy. During the minimization, photonuclear attenuation is found to be important for higher MV beams. For accurate spectral unfolding, Monte Carlo plays an auxiliary but important role in two areas: precalculating the detector energy response, and corrections for certain nonideal attenuation conditions. With the challenges associated with smaller transmission signals, a useful observation is that accurate spectral unfolding can be achieved with a transmission cutoff of only 10%, provided that the other components of the proposed approach are implemented. Finally, the practicality of the proposed approach is successfully demonstrated on a typical clinical linac for 6, 10, and 25 MV beams.

ACKNOWLEDGMENTS

From NRC, the authors thank Carl Ross for useful discussions on the previous NaI measurements, David Marching-

ton for providing the inhouse monitor chamber details, and Frederic Tessier for discussions on his EPOM work and the Elekta BEAMnrc model. Elsayed Ali acknowledges the funding from a Vanier CGS. Dave Rogers acknowledges the funding from the CRC program, NSERC, CFI, and OIT.

[a]Electronic mail: eali@physics.carleton.ca
[b]Electronic mail: malcolm.mcewen@nrc-cnrc.gc.ca
[c]Electronic mail: drogers@physics.carleton.ca

[1]B. A. Faddegon, C. K. Ross, and D. W. O. Rogers, "Forward-directed bremsstrahlung of 10- to 30-MeV electrons incident on thick targets of Al and Pb," Med. Phys. **17**, 773–785 (1990).
[2]B. A. Faddegon, C. K. Ross, and D. W. O. Rogers, "Angular distribution of bremsstrahlung from 15 MeV electrons incident on thick targets of Be, Al and Pb," Med. Phys. **18**, 727–739 (1991).
[3]D. J. Landry and D. W. Anderson, "Measurement of accelerator bremsstrahlung spectra with a high-efficiency Ge detector," Med. Phys. **18**, 527–532 (1991).
[4]A. Ahnesjö and P. Andreo, "Determination of effective bremsstrahlung spectra and electron contamination for photon dose calculations," Phys. Med. Biol. **34**, 1451–1464 (1989).
[5]O. Sauer and M. Neumann, "Reconstruction of high-energy bremsstrahlung spectra by numerical analysis of depth-dose data," Radiother. Oncol. **18**, 39–47 (1990).
[6]D. Sheikh-Bagheri and D. W. O. Rogers, "Monte Carlo calculation of nine megavoltage photon beam spectra using the BEAM code," Med. Phys. **29**, 391–402 (2002).
[7]E. S. M. Ali and D. W. O. Rogers, "An improved physics-based approach for unfolding megavoltage bremsstrahlung spectra using transmission analysis," Med. Phys. **39**, 1663–1675 (2012).
[8]E. S. M. Ali and D. W. O. Rogers, "Functional forms for photon spectra of clinical linacs," Phys. Med. Biol. **55**, 31–50 (2012).
[9]C. R. Baker and K. K. Peck, "Reconstruction of 6 MV photon spectra from measured transmission including maximum energy estimation," Phys. Med. Biol. **42**, 2041–2051 (1997).
[10]P. Francois, F. Coste, J. Bonnet, and O. Caselles, "Validation of reconstructed bremsstrahlung spectra between 6 MV and 25 MV from measured transmission data," Med. Phys. **24**, 769–773 (1997).
[11]T. Shimozato, K. Tabushi, S. Kitoh, Y. Shiota, C. Hirayama, and S. Suzuki, "Calculation of 10 MV x-ray spectra emitted by a medical linear accelerator using the BFGS quasi-Newton method," Phys. Med. Biol. **52**, 515–523 (2007).
[12]W. H. Hinson, W. T. Kearns, A. F. deGuzman, and J. D. Bourland, "Photon spectral characteristics of dissimilar 6 MV linear accelerators," Med. Phys. **35**, 1698–1702 (2008).
[13]A. Nisbet, H. Weatherburn, J. D. Fenwick, and G. McVey, "Spectral reconstruction of clinical megavoltage photon beams and the implications of spectral determination on the dosimetry of such beams," Phys. Med. Biol. **43**, 1507–1521 (1998).
[14]W. H. Hinson and J. D. Bourland, "Spectral reconstruction of high energy photon beams for kernel based dose calculations," Med. Phys. **29**, 1789–1796 (2002).
[15]A. Piermattei, G. Arcovito, L. Azario, C. Bacci, L. Bianciardi, E. De Sapio, and C. Giacco, "A study of quality of bremsstrahlung spectra reconstructed from transmission measurements," Med. Phys. **17**, 227–233 (1990).
[16]A. Catala, P. Francois, J. Bonnet, and C. Scouamec, "Reconstruction of 12 MV bremsstrahlung spectra from measured transmission data by direct resolution of the numeric system AF = T," Med. Phys. **22**, 3–10 (1995).
[17]R. M. Harrison, G. D. Lambert, and C. L. Chapple, "Spectral estimation and contrast calculation in the design of contrast-detail test objects for radiotherapy portal imaging," Phys. Med. Biol. **38**, 545–556 (1993).
[18]P.-H. Huang, K. R. Kase, and B. E. Bjärngard, "Reconstruction of 4-MV bremsstrahlung spectra from measured transmission data," Med. Phys. **10**, 778–785 (1983).
[19]R. G. Waggener, M. M. Blough, J. A. Terry, D. Chen, N. E. Lee, S. Zhang, and W. D. McDavid, "X-ray spectra estimation using attenuation measurements from 25 kVp to 18 MV," Med. Phys. **26**, 1269–1278 (1999).
[20]M. Partridge, "Reconstruction of megavoltage photon spectra from electronic portal imager derived transmission measurements," Phys. Med. Biol. **45**, N115–N131 (2000).
[21]E. S. M. Ali, M. R. McEwen, and D. W. O. Rogers, "Detailed high-accuracy megavoltage transmission measurements: A sensitive experimental benchmark of EGSnrc," Med. Phys. **39**, 5990–6003 (2012).
[22]I. Kawrakow, "Accurate condensed history Monte Carlo simulation of electron transport. I. EGSnrc, the new EGS4 version," Med. Phys. **27**, 485–498 (2000).
[23]I. Kawrakow, E. Mainegra-Hing, D. W. O. Rogers, F. Tessier, and B. R. B. Walters, "The EGSnrc Code System: Monte Carlo simulation of electron and photon transport," NRC Technical Report PIRS-701 v4-2-3-2 (National Research Council Canada, Ottawa, 2011) (available URL: http://www.irs.inms.nrc.ca/inms/irs/EGSnrc/EGSnrc.html).
[24]E. S. M. Ali, M. R. McEwen, and D. W. O. Rogers, "Data for an accurate transmission measurement benchmark," Technical Report CLRP 12–02 (Carleton University, Ottawa, 2012), 15 pp. (available URL: http://www.physics.carleton.ca/clrp/transmission).
[25]M. S. MacPherson and C. K. Ross, "A magnetic spectrometer for electron energy calibration," Technical Report PIRS–0617 (IRS, NRC, Ottawa, 1998), 59 pp. (available URL: http://irs.inms.nrc.ca/publications/reports/pdf/PIRS-0617-1998.pdf).
[26]C. K. Ross, M. R. McEwen, A. F. McDonald, C. D. Cojocaru, and B. A. Faddegon, "Measurement of multiple scattering of 13 and 20 MeV electrons by thin foils," Med. Phys. **35**, 4121–4131 (2008).
[27]B. A. Faddegon, M. Asai, J. Perl, C. Ross, J. Sempau, J. Tinslay, and F. Salvat, "Benchmarking of Monte Carlo simulation of bremsstrahlung from thick targets at radiotherapy energies," Med. Phys. **35**, 4308–4317 (2008).
[28]F. Tessier and I. Kawrakow, "Calculation of the electron-electron bremsstrahlung cross-section in the field of atomic electrons," Nucl. Instrum. Methods Phys. Res. B **266**, 625–634 (2008).
[29]E. S. M. Ali and D. W. O. Rogers, "Implementation of photonuclear attenuation in EGSnrc," Technical Report CLRP 12–01 (Carleton University, Ottawa, 2012), 14 pp. (available URL: http://www.physics.carleton.ca/clrp/photonuclear).
[30]P. R. Almond, P. J. Biggs, B. M. Coursey, W. F. Hanson, M. S. Huq, R. Nath, and D. W. O. Rogers, "AAPM's TG–51 protocol for clinical reference dosimetry of high-energy photon and electron beams," Med. Phys. **26**, 1847–1870 (1999).
[31]R. E. Bentley, *Uncertainty in Measurement: The ISO Guide*, 6th ed. (National Measurement Laboratory CSIRO, Australia, 2003).
[32]E. Tonkopi, M. McEwen, B. R. B. Walters, and I. Kawrakow, "Influence of ion chamber response on in-air profile measurements in megavoltage photon beams," Med. Phys. **32**, 2918–2927 (2005).
[33]D. W. O. Rogers, B. A. Faddegon, G. X. Ding, C.-M. Ma, J. Wei, and T. R. Mackie, "BEAM: A Monte Carlo code to simulate radiotherapy treatment units," Med. Phys. **22**, 503–524 (1995).
[34]D. W. O. Rogers, B. Walters, and I. Kawrakow, "BEAMnrc Users Manual," NRC Technical Report PIRS-509(A) revL (National Research Council of Canada, Ottawa, 2011) (available URL: http://www.irs.inms.nrc.ca/BEAM/beamhome.html).
[35]I. Kawrakow, E. Mainegra-Hing, F. Tessier, and B. R. B. Walters, "The EGSnrc C++ class library," Technical Report PIRS–898 (rev A) (National Research Council of Canada, Ottawa, 2009) (available URL: http://www.irs.inms.nrc.ca/EGSnrc/PIRS898/).
[36]I. Kawrakow, D. W. O. Rogers, and B. Walters, "Large efficiency improvements in BEAMnrc using directional bremsstrahlung splitting," Med. Phys. **31**, 2883–2898 (2004).
[37]D. W. O. Rogers, "Analytic and graphical methods for assigning errors to parameters in non-linear least squares fitting," Nucl. Instrum. Methods **127**, 253–260 (1975).
[38]D. W. Marquardt, "An algorithm for least-squares estimation of nonlinear parameters," SIAM J. Appl. Math. **11**, 431–441 (1963).
[39]M. J. Berger, J. H. Hubbell, S. M. Seltzer, J. Chang, J. S. Coursey, R. Sukumar, D. S. Zucker, and K. Olsen, "XCOM: Photon cross section database (version 1.5)," Technical Report (NIST, Gaithersburg, MD, 2010) (available URL: http://physics.nist.gov/xcom).
[40]International Atomic Energy Agency, "Handbook of photonuclear data for applications: cross sections and spectra," Technical Report TECDOC 1178 (IAEA, Vienna, Austria, 2000) (available URL: http://www-nds.iaea.org/photonuclear).
[41]F. Tessier and I. Kawrakow, "Effective point of measurement of thimble ion chambers in megavoltage photon beams," Med. Phys. **37**, 96–107 (2010).
[42]F. Tessier (personal communication, 2012).